The mineral exploration of rare earth elements using the optimal sampling pattern in the Baghak mine

Seyyed Saeed Ghannadpour[a, *], Ardeshir Hezarkhani[a]

[a] *Department of Mining Engineering, Amirkabir University of Technology (Tehran Polytechnic), Tehran, Iran.*

ABSTRACT

In the current study, sampling from the Baghak anomaly in the Sangan mines has been carried out based on radioactivity and radiation measurement methods. This study aims to survey the presence or absence of such a relation (between rare earth and radioactive elements) in a skarn mine which is a different case study in central Iran. Mineralogical studies (based on optical and electronic microscopic observations), univariate and multivariate statistical investigations, and geochemical analyses have been applied. Results show that the Baghak anomaly is due to a significant amount of U, Ce, La, and a high concentration of REEs. It seems that the mineralization of Th and REEs occurred simultaneously with the formation of iron skarn, while uranium mineralization in hydrothermal form occurred in a secondary phase after the skarn iron mineralization. Finally, it could be acknowledged that in addition to the presence of such a relation in the mineralization (central Iran mineralization), there is an acceptable correlation between these elements in the Baghak iron-skarn mineralization.

1. Introduction

The existence of REEs in the Sangan iron ore mine; is known as an important skarn mine in Khorasan Razavi province, Iran (at the eastern edge of the Sabzevar-Dorouneh magmatic belt (SDMB)). The concentration of REEs in garnets from the Sangan iron mine was measured by LA-ICP-MS (Boomeri, 1998; 2006). The Sangan and eastern anomalies of Ferezneh and Senjedak-I were reported (Mazhari et al. 2015; 2016; 2017). The ratio of LREE/HREE in Ferezneh changed from 58.2 to 78.13. Additionally, moderate enrichment of LREE and a positive anomaly of Eu were observed (Mazhari et al., 2015). In Senjedak-I, REEs show an Eu negative anomaly, a moderate enrichment of LREE, a positive pattern close to flat HREE, and negative anomalies of Ba, Sr, La, Ce, Ti, and Eu (Mazhari et al., 2016). The enrichment of HFSE, Zr, Nb, Ga, Ta, Y, and Hf and the depletion of Ba and Sr were related to post-orogenic granitoids in some eastern anomalies (Golmohammadi et al., 2014). A relative enrichment of LREE in proportion to HREE and enrichment of LILE in proportion to HFSE elements in intrusive bodies show the formation of magma in a subduction zone in some western and central anomalies (Malekzadeh Shafaroudi et al., 2013; Golmohammadi et al., 2013; 2015).

It is also noteworthy that the association and enrichment of REEs are recognized as a common feature in most prospecting points of uranium that belong to the atomic energy organization of Iran (AEOI) and particularly the central Iran zone. Sometimes, the association of these elements with U by values greater than its economic limit has caused genetic modelling of U-REE, the exploration geochemistry analysis and mineral processing studies of these elements in the semi-industrial phase are taken into consideration in parallel processes (Ghannadpour, 2014).

In this study, according to the importance of REEs, evidence of their existence in the Sangan mine, and the observed relation in many studies which are carried out by AEOI, this relation has been investigated in more detail in the case of a Fe-skarn mineralization in the Baghak anomaly which is located in Sangan iron mines as a different mineralization from the central Iran mineralization. The radiation feature was applied for the first time in this study to achieve an optimized sampling with a low cost for prospecting REEs and sampling was carried out based on the radiation feature of samples using spectrometry.

2. Geology

The Sangan iron skarn deposit at the Khorassan department in northeastern Iran is located at the eastern edge of the Khaf-Kashmar-Bardaskan volcano-plutonic-metallogenic belt (KKB-VPMB) (Fig. 1) Having a proven reserve of over 1000 Mt iron ore (53 % Fe), Sangan represents a world-class iron skarn deposit. The KKB-VPMB is an arcuate, W–E to NW–SE trending, Cenozoic volcano-plutonic arc of 400 km extension and 50 km width along the major Doruneh Fault that separates the KKB-VPMB from the southerly Lut Block (Fig. 1). Numerous iron, copper, and gold deposits and occurrences (e.g., Kuh-e-Zar, Shahrak, Tannurjeh, Sangan) indicate that the KKB-VPMB is a metallogenic belt of great economic potential. The actual regional tectonomorphology results from the final Alpidic orogenesis, whereas the main lineaments and the general strike of the mountain ranges reflect the reactivation of the earlier Assyntic orogenic structures. The two blocks of Sabzevar in the north and Lut in the south of the Doruneh Fault show dextral and sinistral movements in different periods with the dextral movement being the last movement. The structural features of the region such as faults and foldings, as well as the strike of the formations, follow the NW–SE to E–W direction of the major Doruneh Fault. A series of NW–SE striking faults (N150) with sinistral and dextral movements, including the main Dardvey fault, have affected the

---

* Corresponding author. *E-mail address:* s.ghannadpour@aut.ac.ir (S. S. Ghannadpour).

Sangan prospect and have split the orebodies (Golmohammadi et al. 2015).

The Sangan prospect is dominated by the Cenozoic felsic subvolcanic intrusions and volcanic rocks, as well as thick, weakly metamorphosed siliciclastic sedimentary rock successions of Jurassic age, and Cretaceous carbonate rocks. Magmatism at the Sangan area commenced with the eruption of volcanic rocks and was closely followed by the emplacement of granitoid porphyries consisting of granite, granodiorite, monzonite, diorite, and alkali feldspar granites (syenite, syenogranite, etc.) plutons, stocks, and dikes. Crosscutting relationships and the absence or presence of skarn mineralization at the contact of the intrusions, suggest that the monzonite to quartz monzonites/syenites were emplaced before the mineralization took place. The quartz alkali syenite to quartz syenite and the syenogranites exhibit iron skarn mineralization at their contact and are here assigned as the source intrusions. Volcanic rocks are largely exposed in the southern parts of the Sangan district and mainly consist of acid to intermediate and occasionally mafic rocks that are composed of rhyodacite, dacite, andesite–dacite, andesite, pyroxene andesite to basalt. Jurassic formations are the oldest geological units that outcrop in the central mine areas where they strike E–W, and consist of shale and sandstone that are silicified at the contact with Cenozoic intrusions (Fig. 2) (Golmohammadi et al. 2015).
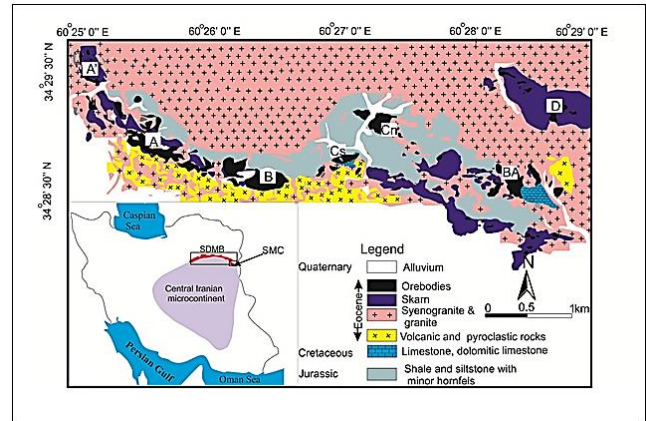

Fig. 2. Map of Iran and geological map of the Sangan region including the location of the Sangan deposit and the Eocene plutonic and volcanic rocks based on 1:250,000 geological maps of the Taybad (Alavi Naini, 1982). Locations of A, A', B, Cn, Cs, D, and BA (Baghak) skarn types are shown (Sepidar et al. 2017).

3. Sampling and Methodology

The Baghak magnetite iron ore deposit is one section of the giant Sangan iron ore mines. Baghak and Dardevey deposits are located in the central part of the Dardvey-Baghak fault which has dislocated these two deposits for less than one kilometer. According to field observations, petrographical, mineralogical, and geochemical studies, the genesis of this iron ore deposit is proposed to be the Skarn type. Recent studies have indicated that the deposit is a magnetite Fe-oxide deposit from the IOCG deposit group (Ghannadpour et al. 2018).

The Sangan Magnetite Complex (SMC) has performed drilling (239 exploratory boreholes) in the Baghak area from the beginning of exploration at the deposit. Coring and chemical analysis produced elemental concentration data for Fe, S, and FeO in weight percent (Iran Eastern Iron Ore Co, 2011; Ghannadpour et al. 2018). The samples have been collected by researchers in SMC and were analyzed by wet chemistry method and wave-length dispersive X-ray fluorescence spectrometry on a LECO CS-230 XRF spectrometer at the central laboratory of the Sangan iron ore complex (Golmohammadi et al. 2015). The 3D view of boreholes is depicted in Fig. 3.
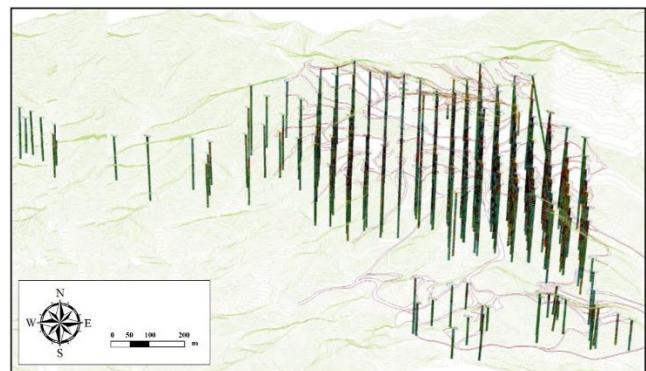

Fig. 3. Three-dimensional display of drilled boreholes in Baghak mine.

Sampling operation has been carried out from drilling cores in view of the relation between REEs and radioactive elements. Potential radioactive spaces and significant P-bearing cores (based on geochemical analysis of drilling cores) are the base of sampling. Sampling is divided into two parts:

Sampling operation has been carried out from drilling cores in view of the relation between REEs and radioactive elements. Potential radioactive spaces and significant P-bearing cores (based on geochemical analysis of drilling cores) are the base of sampling.
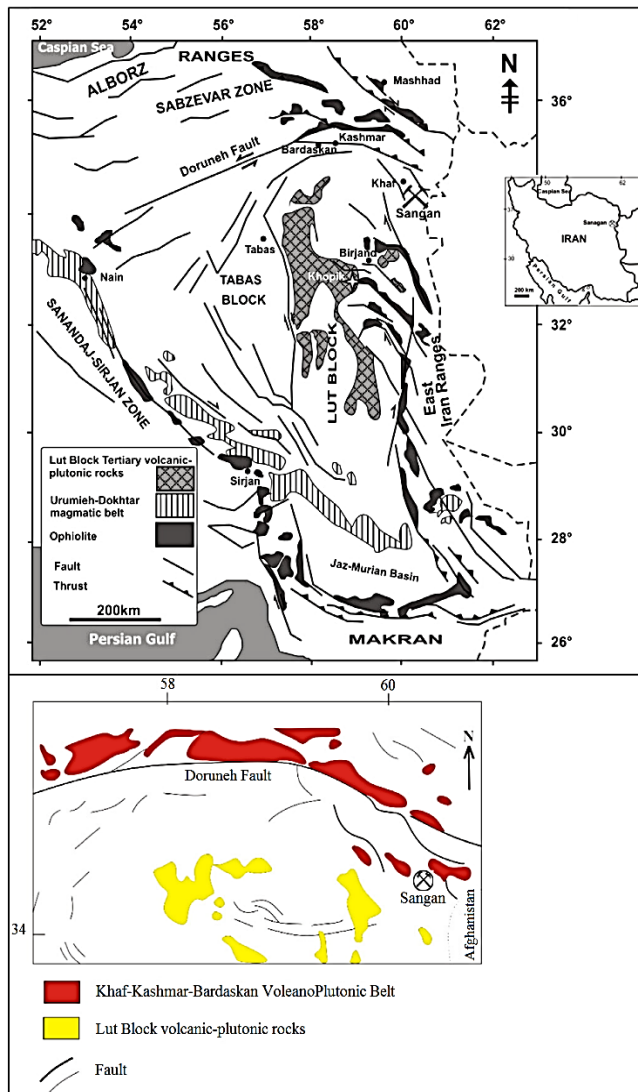

Fig. 1. Simplified structural map of eastern Iran showing the location of the Sangan deposit at the eastern edge of Doruneh Fault, the KKB–VPMB, and the southerly Cenozoic volcano-plutonic rocks of the Lut Block (Golmohammadi et al. 2015).

Sampling is divided into two parts:

Part I: applying logs from some boreholes.

It is noteworthy that the logging was carried out only in 24 boreholes of the Baghak anomaly and direct radiometry seems essential for detailed surveying of the relation between radioactivity and REEs.

And part II: direct spectrometry operation of drilled cores and selecting radioactive samples using a portable hand-held spectrometer, RS 230 manufactured by Radiation Solutions Inc., Canada.

First, the maximum CPS using logs from each borehole is specified and high values are determined for sampling (Fig. 4). Then, the boreholes which should be more investigated are determined along with the length of maximum radioactivity. That way the boreholes with radioactivity less than 1000 CPS are in second priority for hand radiometry and boreholes with a higher radioactivity than 1000 CPS are applied in first priority for validating logging results, obtaining primary information from the study area, and starting sampling operation.

Then, in the first step of sampling in the core-sample warehouse, determined boreholes are referred and spectrometry is carried out in considered length or maybe throughout the borehole. After preliminary surveying of drilled cores, primary information, including background and desired radioactivity of the study area, is determined. Those mentioned values are presented in Table 1.

In the next step, according to the obtained information, regular and detailed radiometry and sampling are carried out. First, logged boreholes with radioactivity higher than 1000 CPS are investigated, and then, non-logged boreholes are considered and samples are taken from the points by the higher relative radioactivity. Finally, for a better display of the presence or absence of relation between REEs and radioactive elements, some samples are taken from phosphorous cores and parts that involve minimum radioactivity. It is noteworthy that samples are not taken from points and totally, 151 samples in different intervals from unit length (by the center of maximum radioactivity) are taken (from 10 cm to 3 m).

4. Preliminary Investigation

In this section, the resulting data from spectrometry operation (radiometry) is investigated before describing the preparation and detailed study of the samples taken in the previous section. First, the boreholes which show suitable radioactivity or include a significant value of P according to their analyses are determined, and then, for a detailed study of the relation between REEs and radioactive elements, samples are ordered based on radioactivity (measured by spectrometer) and first the 47 samples along with 3 samples from borehole BK25 including high P concentration were selected for microscopic studies. Fig. The boreholes of the 47 mentioned samples (radioactivity of greater than 950 CPS) were shown in Fig. 5.

Radioactive boreholes and general radioactivity in the Baghak anomaly strike NW-SE (Fig. 5). As a matter of fact, the radioactivity trend of the study area follows the faulting strike in the Sangan mine which is particularly coincident with the fault located in northern C anomaly (Ghannadpour and Hezarkhani, 2021; 2022). This fact increases the probability of radioactive element-bearing mineralization along the faults located in the study area.

Then, the radioactivity of samples is considered as the base of selecting them for providing thin sections and microscopic studies (using an optical microscope (Leitz German make) and electronic microscope (SEM XL30, Philips, Netherlands)). For this purpose, the rock which includes maximum radioactivity in each sample bag is selected using a scintillometer (SPP2 manufactured by SAPHYMO, France) for providing thin and polished sections. Before providing the sections, samples are studied macroscopically and the results are available in Table 2.

5. Optical microscope studies

From selected samples in the previous section, 24 polished sections and 27 thin sections are provided and the section type for each sample

is available in Table 2. However, according to the significant similarity of samples and results, and also the limitation of the page number, results relative to only four sections (thin sections: 94-EXP-SN-34-16 and -43-20 and polished sections: 94-EXP-SN-30-12 and -34-16) are presented in this section.

Microscopic images of 94-EXP-SN-43-20 and 94-EXP-SN-34-16 thin sections are shown in Figs. 6 and 7 respectively.

Microscopic images of polished sections (94-EXP-SN-30-12 and -34-16) are also illustrated in Figs. 8 and 9.

No evidence of the presence of REE-bearing minerals, such as monazite, bastnaesite, apatite, or xenotime, was found under the microscope (e.g., Figs. 6, 7, 8, and 9). Also, identifying the radioactive element-bearing minerals like uraninite, was not possible with an optical microscope. However, it should be noted that a significant amount of sphene and allanite was observed as a network of fine to coarse minerals in most of the sections (Figs. 10 and 11).

Allanite belongs to the epidote group and its general formula is $Ca_2(Al, Fe)_3(OH)(SiO_4)_3$ (Rabadjieva et al., 2009). Fe, Ce, and Al cations can substitute in the allanite structure under particular conditions and allanite is represented by the formula of $(Ca, Fe^{2+})_2(Al, Ce, Fe^{3+})_2(OH)(SiO_4)_3$ (Ercit, 2002; Gregory et al., 2007; Guastoni et al., 2017). Thus, it can be probable that allanite (or sphene) hosts REEs like Ce in the study area.

Diamond-shaped minerals were observed in this section (Fig. 11a). According to the apparent features of these minerals, the presence of monazite in this section was probable. However, due to the similarity of this mineral and to sphene (Gribble, 1988) which is observed abundantly in all sections, SEM studies seemed more necessary.
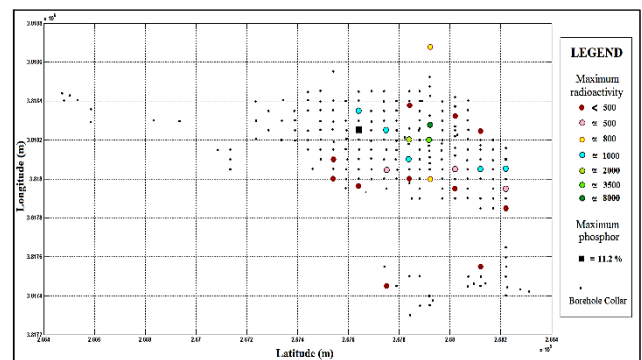

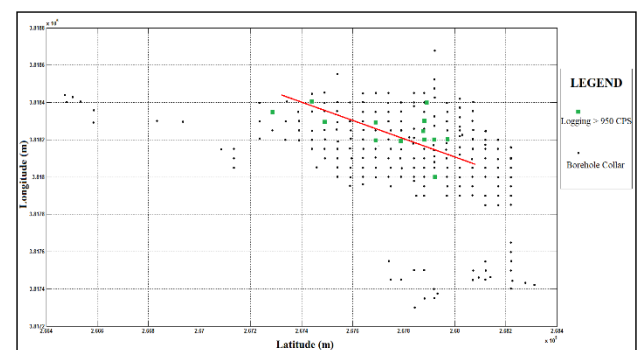**Fig. 4.** Map of showing the maximum radioactivity of boreholes on their collars.

Fig. 5. Map showing boreholes that include radioactivity of more than 950 CPS (red line: radioactivity trend in the region).

Table 1. Basic information on the study area.

Background radioactivity (CPS)	Radioactivity in the core library (CPS)	Optimal radioactivity threshold (CPS)
200-250	250-300	800

Table 2. Petrology and radioactivity of selected samples for preparation of sections (thin sections and polished blocks).

| Sample ID	CPS	Section type		Petrology
		Thin	Polish	
94-EXP-SN-01-01	350	*	*	Magnetite-Pyrite-Amphibole?
94-EXP-SN-08-02	100	*	*	Pyrite-Amphibole?
94-EXP-SN-09-03	80-100	*	*	Magnetite-Pyrite
94-EXP-SN-10-04	100	*	*	Carbonate
94-EXP-SN-11-05	250	-	*	Magnetite-Amphibole?
94-EXP-SN-14-06	300	*	*	Calcite-Pyrite-Amphibole-Pyroxene-Magnetite
94-EXP-SN-15-07	250-300	*	*	Phlogopite-Biotite-Pyrite-Feldspar
94-EXP-SN-17-08	250-300	*	*	Pyrrhotite?-Amphibole?
94-EXP-SN-22-09	250-300	*	*	Magnetite-Pyrite-Feldspar-Amphibole?
94-EXP-SN-24-10	300	*	*	Pyrite -Silica -Biotite
94-EXP-SN-25-11	300	*	*	Pyrite-Amphibole-Pyroxene
94-EXP-SN-30-12	200-230	-	*	Pyrite-Magnetite-Carbonate
94-EXP-SN-31-13	220	*	-	Magnetite
94-EXP-SN-32-14	200	*	*	Carbonate-Chloride-Amphibole
94-EXP-SN-33-15	150	*	*	Magnetite-Pyrite-Amphibole-Pyroxene
94-EXP-SN-34-16	300	*	*	Pyrite-Magnetite-Calcite
94-EXP-SN-36-17	320	*	-	Magnetite-Pyrite
94-EXP-SN-37-18	150	*	*	Amphibole-Chloride-Magnetite
94-EXP-SN-40-19	300	*	*	Magnetite-Pyrite
94-EXP-SN-43-20	1000	*	*	Magnetite-Pyrite-Amphibole minerals?
94-EXP-SN-45-21	400	*	*	Magnetite-Pyrite-Amphibole minerals?
94-EXP-SN-46-22	300	*	-	Magnetite-Amphibole minerals?
94-EXP-SN-49-23	200	*	*	Carbonate-Silica-Phlogopite
94-EXP-SN-50-24	200	*	*	Phlogopite-Biotite-Carbonate-Pyrite
94-EXP-SN-22-25	250-300	*	*	Carbonate-Amphibole
94-EXP-SN-25-26	300	-	*	Pyrite-Carbonate-Amphibole minerals
94-EXP-SN-17-27	250-300	*	-	Pyrite-Carbonate-Silica
94-EXP-SN-17-28	250-300	*	-	Phlogopite-Biotite-Amphibole-Pyrite
94-EXP-SN-15-29	250-300	*	-	Phlogopite-Biotite-Carbonate
94-EXP-SN-50-30	250	*	-	Phlogopite-Magnetite-Amphibole
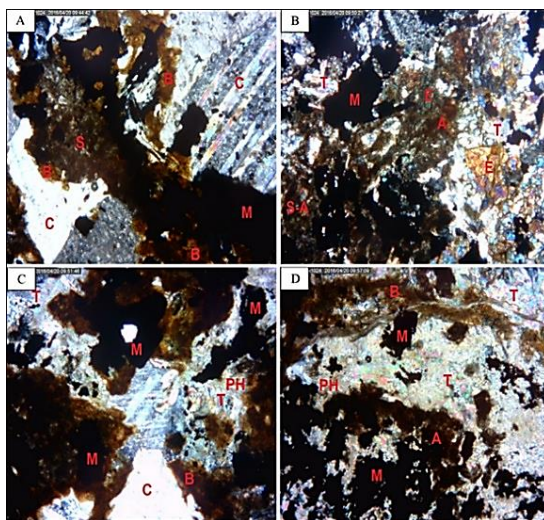
Fig. 6. Images of thin section 94-EXP-SN-34-16. A: large and amorphous minerals of sphene in keeping with magnetite and biotite along with them and also coarse skarn carbonate minerals, B: the presence of epidote, sphene-epidote-allanite and allanite as a set-in association with magnetite (medium-grained magnetite). talc within epidote minerals and along with magnetite, C: coarse skarn carbonate minerals and biotitization in the form of coarse minerals overlapping on the magnetite and sphene. D: the presence of allanites beside magnetite and displaying biotite veinlets and phlogopitization of talc. (B = biotite, C = carbonatite, S = sphene, M = magnetite, T = talc, E = epidote, S-A = sphene-allanite, A = allanite, PH = and Phlogopite).
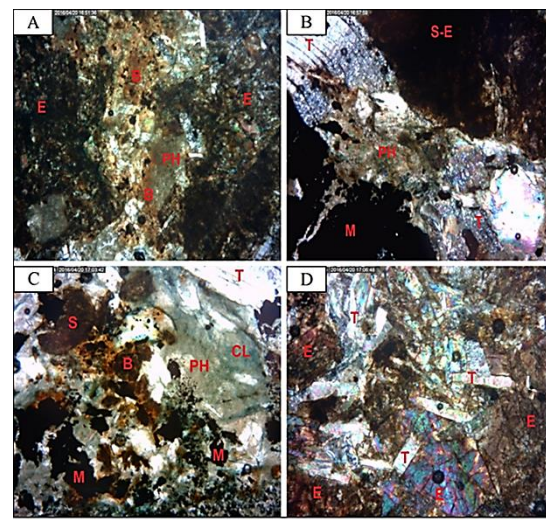

Fig. 7. Images of thin section 94-EXP-SN-43-20. A: A set of epidotes is seen on both sides. Biotite is formed in the middle on carbonate and phlogopite with fine texture is seen along with it, B: A set of sphene-epidote and coarse talc is likely resulted from silicatization of carbonate and also phlogopite overlapped on them and magnetite are seen, C: phlogopite-carbonate which has been chlorinated in some parts and scattered talc minerals are seen in it and finally their accompaniment by small minerals such as sphene and magnetite. D: the accumulation of epidote minerals associated with dispersed talc. A fine-grained phlogopite is seen in overlapping on the carbonate. (T = talc, S = sphene, B = biotite, M = magnetite, PH = phlogopite, E = epidote, S-E = sphene-epidote, CL = chlorite.
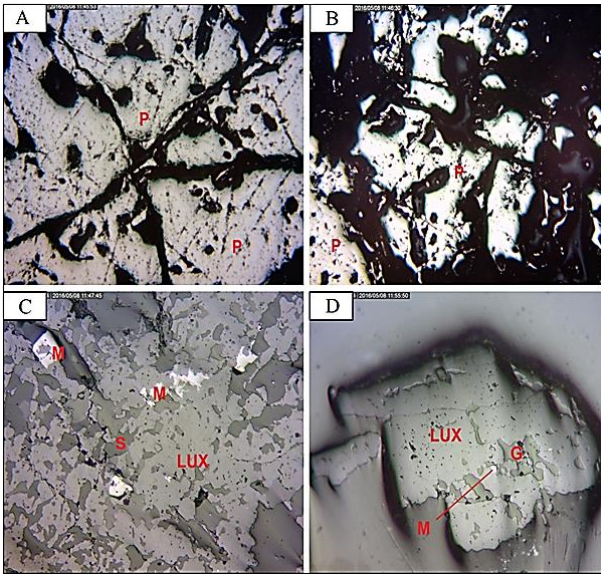
Fig. 8. Images of polished section 94-EXP-SN-30-12. A: pyrite. Corrosion in the site of the cracks and their intersections is relatively severe. B: severe corrosion and fine-grained corrosion texture is seen in pyrite. C: leucoxene areas along with leakage of gangue to inside it which the small magnetite minerals are dispersed in them. The leakage of gangue to the inside of the magnetite is seen. D: succession leucoxene is seen instead of titanium-magnetite and also small magnetite minerals are seen as the remaining texture. There are gangue leakages into leucoxene (G = gangue, M = magnetite, LUX = leucoxene, P = pyrite, S = sphene)
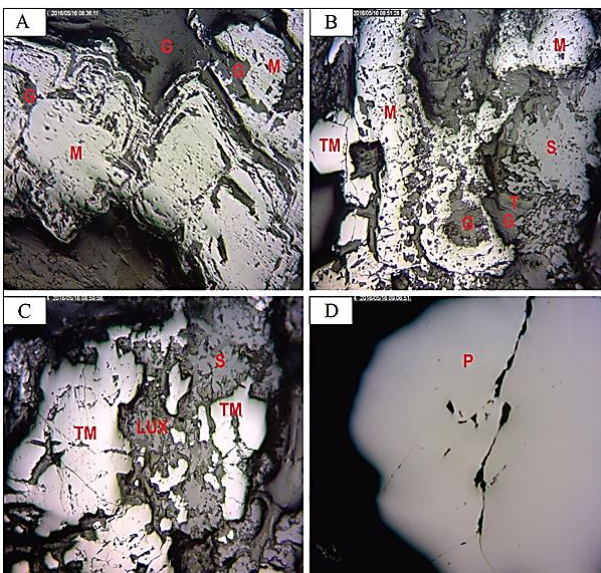

Fig. 9. Images of polished section 94-EXP-SN-34-16. A: the presence of coarse magnetite with corrosion texture (fine-grained) and the leakage of gangue to parallel of cleavages and its outer boundary, B: magnetite with fine-grained corrosion texture and the leakage of gangue to its outer boundary. The magnetite is located within the gangue and sphene minerals are seen next to it and finally, in left side, magnetite includes titanium with corrosion texture, C: titanomagnetite with delicate corrosion texture that leucoxene has been formed from its alteration (in the central image) and the remaining magnetite as amorphous minerals are seen in leucoxene, D: Subhedral crystal of pyrite with delicate corrosion texture that includes cracks and crevices. (G = gangue, M = magnetite, TM = titanium magnetite, T = talc, S = sphene, LUX = leucoxene, P = pyrite).

Identifying mentioned minerals become easier and the existing doubt can be removed by one scan and simple investigation in SEM studies, and measuring P, Ca, Ti, and Si values. Phosphorus is involved in monazite ((REE) PO_4), but sphene ($CaTiSiO_5$) includes no P and in

addition, Ca, Ti, and Si are involved in that (Gregory et al., 2007). Finally, a detailed study of sections by SEM is carried out in the AUT SEM laboratory.

6. SEM Study Results

In Fig. 12, after U scanning by the microscope, it was revealed that the light spot in figures (Figs. 12; 13. A, B) corresponded to U-bearing minerals.

According to Figs. 13. C and 14.D, it is observed that the lighter mineral (Figs. 13. A, B; 14. A, B, and C) is corresponded to Fe (magnetite) and surrounding minerals (dark and light grey colored minerals) based on a significant amount of Si (Figs. 13.D; 14. G), Ca (Figs. 13. E; 14. F) and Al (Fig. 14. H) corresponds to epidote. It could be noted that Ce is located in the structure of epidote (allanite) in this study (Figs. 13. F; 14. E). Therefore, surrounding minerals (dark and light grey colored minerals) in Fig. 13. A and 16. A, B, and C are considered as allanite. As it is observed, U is displayed in the REEs-bearing minerals (allanite).

According to Fig. 14 and 15 due to the more specific gravity of U compared to other elements like Fe, U is lighter than the others. This is true in the case of Fe and other elements, and also other minerals. In Fig. 13 and 14, Fe is displayed as lighter than the other elements and minerals.

In this section, by studying and investigating the first thin section, the probability of the presence of REEs in allanite is highlighted. Thus, studying other sections will be efficient in confirming this probability. After SEM studies on polished sections of 94-EXP-SN-30-12 and -34-16, several photos are captured from different locations of the section (Fig. 15, 16, and 17) which are going to be discussed in the following.
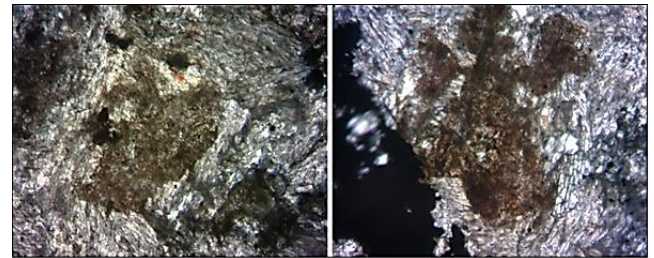

Fig. 10. Zones contain allanite which are determined for SEM analysis (thin section 94-EXP-SN-01-01)
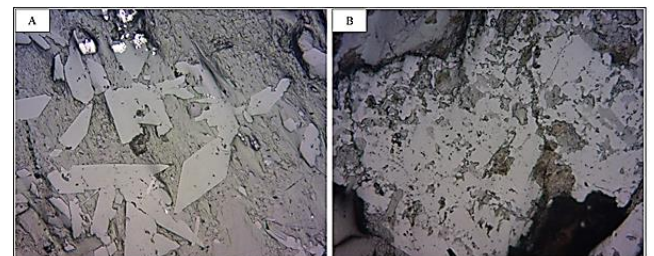

Fig. 11. Zones contain allanite and sphene in polished sections. A: allanite and sphene minerals (polished section 94-EXP-SN-30-12), and B: sphenes which are similar to monazite (94-EXP-SN-34-16)
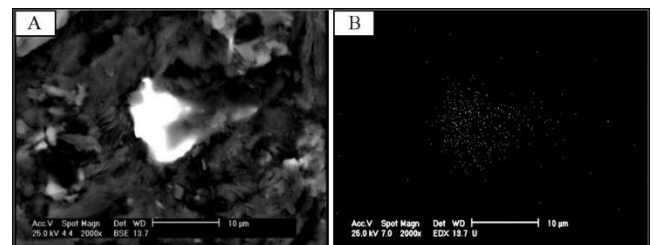

Fig. 12. A. Uranium in thin section 94-EXP-SN-43-20, B: scanning for uranium at the scale of 10 microns from part A.
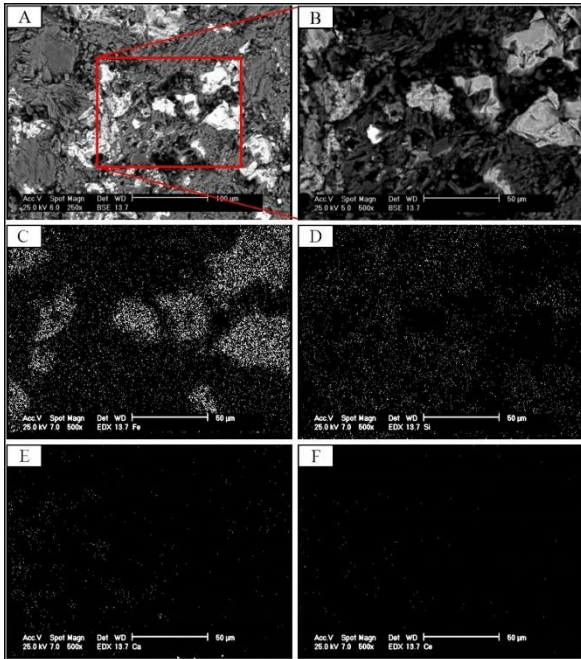
Fig. 13. A: Displaying uranium, iron, and allanite in thin section 94-EXP-SN-43-20, B: magnification from part A, C: scan result for Fe, D: scan result for Si, E: scan result for Ca, F: scan result for Ce.

In Fig. 15.D, after U scanning by the microscope, it was revealed that the light spots in these figures (Fig. 15. A, B, and C) are corresponded to U-bearing minerals. The scanning process was again performed for two Fe and S elements (Fig. 15. E and F). As seen in this figure, minerals that are located next to uranium (15.A, B, and C) are likely to be pyrite or pyrrhotite, due to the presence of iron and sulfur. The probability of pyrite is more than that of pyrrhotite due to the low amount of sulfur scanned by the microscope. Therefore, as it is observed, U is displayed in the Fe-bearing minerals. Moreover, results show the presence of La (Fig. 16G) and Nd (Fig. 16H) based on scans that were carried out on the dark and light grey colored minerals (16A).

Finally, diamond-shaped minerals which are observed in this section and caused doubt about the presence of monazite, are investigated and SEM back scatter image(Fig. 17) along with a brief description is presented in the following.

No evidence for the presence of monazite was observed in REE scanning results from shaped minerals that were assumed to be probably monazite before (Fig. 11A and Fig. 17). In other words, the result of P-scanning in shaped minerals was negative. Therefore, according to microscopic studies, it was confirmed that shaped minerals correspond to sphene. Light spots are determined to be Fe-bearing minerals according to the Fe-scanning. Finally, it could be said that REEs, especially Ce are present in the samples (Lanthanum and neodymium are also observed in a section) and they have been aggregated as solid solution in allanite minerals. Moreover, it is seen that uranium has been mostly trapped as inclusions in empty spaces of allanite (Fig. 15) and also Fe-bearing minerals (Fig. 17).

7. Geochemical Analysis of Samples

After providing and studying sections, residuals of considered rocks are returned to the bag of each sample, and samples are packed and sent to the Zarazma laboratory (Tehran, Iran) for ICP-MS analysis. ICP-MS analysis by different detection limits for various elements are carried out for each sample and the concentration of 56 elements for each case is reported. The elements along with their detection limits are presented in Table 3. In the following, preparing samples and then their primary statistical analyses for investigating the correspondence between REEs and radioactive elements are discussed computationally.

Fig. 14. A: Displaying allanite and iron in thin section 94-EXP-SN-01-01, B: magnification from part A, C: magnification from part B, D: scan result for Fe, E: scan result for Ce, F: scan result for Ca, G: scan result for Si, H: scan result for Al.
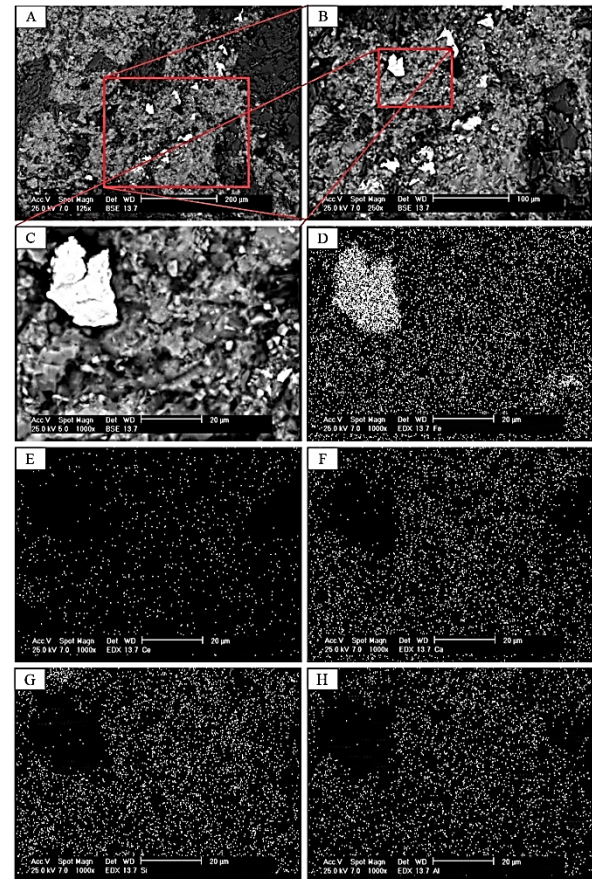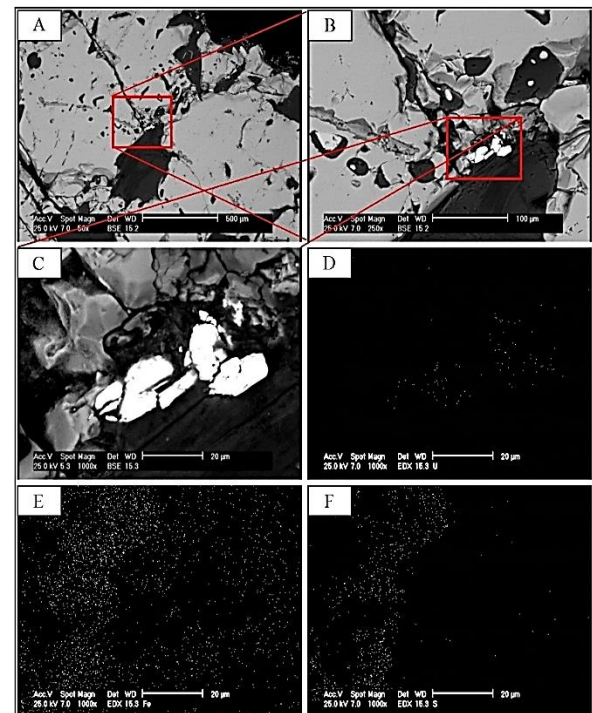

Fig. 15. A: Displaying uranium and iron in polished section 94-EXP-SN-30-12, B: magnification from part A, C: magnification from part B, D: scan result for U, E: scan result for Fe, F: scan result for S.

Table 3. Elements measured using ICP-MS along with its detection limits.

| Element	Cu	Cs	Cr	Co	Ce	Cd	Bi	Be	Ba	As	Al	Ag
DL	1	0.5	1	1	0.5	0.1	0.1	0.2	1	0.1	100	0.1
Unit	ppm	ppm	ppm	ppm	ppm	ppm	ppm	ppm	ppm	ppm	ppm	ppm
Element	Mo	Mn	Mg	Lu	Li	La	In	Hf	Gd	Fe	Eu	Er
DL	0.1	5	100	0.1	1	1	0.5	0.5	0.05	100	0.1	0.05
Unit	ppm	ppm	ppm	ppm	ppm	ppm	ppm	ppm	ppm	ppm	ppm	ppm
Element	Sn	Sm	Se	Sc	Sb	S	Pr	Pb	P	Ni	Nd	Nb
DL	0.1	0.02	0.5	0.5	0.5	50	0.05	1	10	1	0.5	1
Unit	ppm	ppm	ppm	ppm	ppm	ppm	ppm	ppm	ppm	ppm	ppm	ppm
Element	Zn	Yb	Y	W	V	U	Tl	Ti	Th	Te	Tb	Ta
DL	1	0.05	0.5	1	1	0.1	0.1	10	0.1	0.1	0.1	0.1
Unit	ppm	ppm	ppm	ppm	ppm	ppm	ppm	ppm	ppm	ppm	ppm	ppm
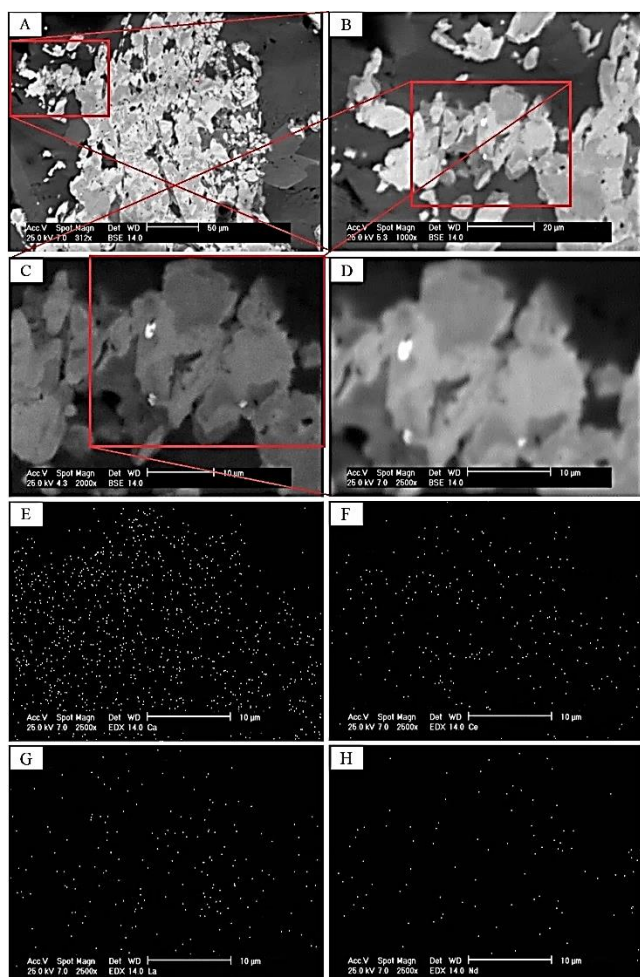
Fig. 16. A: Displaying allanite in thin section 94-EXP-SN-34-16, B: magnification from part A, C: magnification from part B, D: magnification of part C, E: scan result for Ca, F: scan result for Ce, G: scan result for La, H: scan result for Nd.

Fig. 17. A: Displaying sphene minerals and iron in thin section 94-EXP-SN-34-16, B: magnification from part A, C: scan result for Fe.

8. Analyzing the Results

For analyzing the results, investigating the presence or absence of any relation between REEs and radioactivity or radioactive elements, data resulted from geochemical analysis are processed in this section. First, statistical pre-processing is carried out on the geochemical data, and after determining primary statistical characteristics (univariate statistical analysis), the presence or absence of correspondence is considered between radioactivity and REEs, and anomalous variables are determined using multivariate statistical studies.
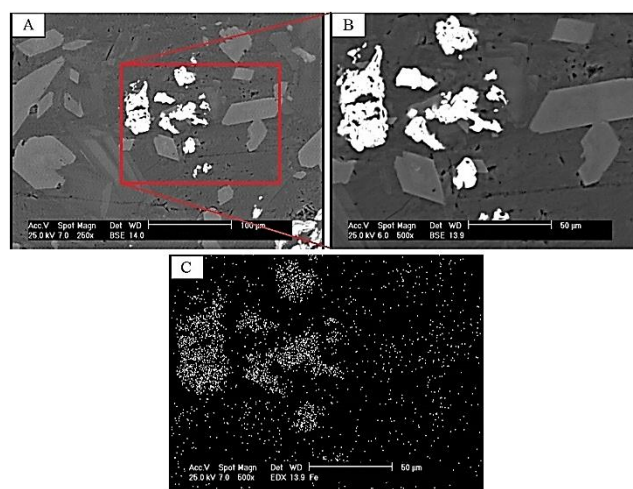
8.1. Geochemical Data Pre-processing

For statistical processing of investigating elements in Baghak study area (151 samples), first the incorrect cases (possible additional characters, outliers or any typos in the data which cause problems in computations) are corrected in data files. Then censored data are replaced by appropriate values (according to lower detection limit reported in Table 3). If censored data involved low number of total (less than 15%), they are replaced by 0.75 of the device detection limit, otherwise, due to inappropriate effects of these elements on the results of statistical analysis, foresaid elements are removed. There is a complete report on removing and replacing censored data in Table 4.

As can be seen in Table 4, two elements of Sc and Fe are removed from statistical analysis due to involving more than 15% of censored data. Therefore, other elements are studied in the following. Then, anomalous values are investigated as outliers. However, due to prevent losing the worth of anomalous values (according to the sensitivity of losing anomalous values as outliers), it was avoided to remove outliers. Because determined outliers do not seem unreasonable and they can be considered as high-grade values.

8.2. Univariate Analysis

After correcting and preparing geochemical data, a weighted average of grade for 151 investigating samples (Without ignoring non-mineralized samples taken for investigating the relation between REEs and radioactivity) and also mineralized samples are calculated and presented in Table 5. According to Table 5, radioactivity in the study area only originated from Uranium, and considering the high concentration of REEs, their correspondence seems more apparent. Actually, this relation is going to be studied in detail by univariate analyses and computing correlation in the following.

Table 4. Characteristics of censored data about the considered elements in Baghak anomaly of Sangan.

Element (ppm)	DL	Type of DL	Number of censored data	Percent of censored data	Replacement condition	Replacement value
U	0.1	Below	0	0	Yes	0.075
Th	0.1	Below	0	0	Yes	0.075
K	100	Below	1	0.66	Yes	75
Fe	100000	Above	123	81.46	No	-
Sc	0.5	Below	41	27.15	No	-
Y	0.5	Below	0	0	Yes	0.375
La	1	Below	0	0	Yes	0.75
Ce	0.5	Below	0	0	Yes	0.375
Pr	0.05	Below	5	3.31	Yes	0.0375
Nd	0.5	Below	0	0	Yes	0.375
Sm	0.02	Below	3	1.97	Yes	0.015
Eu	0.1	Below	7	4.64	Yes	0.075
Gd	0.05	Below	0	0	Yes	0.0375
Tb	0.1	Below	7	4.64	Yes	0.075
Dy	0.02	Below	0	0	Yes	0.015
Er	0.05	Below	0	0	Yes	0.0375
Tm	0.1	Below	5	3.31	Yes	0.075
Yb	0.05	Below	6	3.97	Yes	0.0375
Lu	0.1	Below	14	9.27	Yes	0.075

Table 5. Primary statistical characteristics of considered elements in the Baghak district.

Element	The average grade of total samples (ppm)	The average grade of mineralized samples (ppm)	Maximum grade (ppm)
U	185.62	259.84	923.8
Th	25.93	33.36	138.42
K	14454.14	15841	50284
Y	35.34	43.92	145.7
La	958.76	1276.68	6308
Ce	1125.86	1512.03	6566
Pr	99.91	135.95	605.87
Nd	262.48	365.23	1394.2
Sm	23.36	31.43	126
Eu	4.39	5.87	29.16
Gd	18.75	25.09	91.16
Tb	2.16	2.85	12.37
Dy	8.82	11.38	40.96
Er	4.27	5.35	18.15
Tm	0.53	0.65	2
Yb	3.28	4.22	16.7
Lu	0.44	0.56	1.9
∑ REE	2548.37	3412.2	15312.23

The distribution of all elements is investigated for computing the correlation between their grades in the study area. Then, if the data are not normally distributed, different techniques and transformations are applied for normalizing. Finally, according to considering data distribution, the correlation method is selected and calculated.

Identical composites should be considered for the length of investigating samples and then, detailed analysis can be carried out. The greatest common divisor of the length of samples is considered as the criterion length and samples are extended to 5 cm length composites. The result is generating 2257 samples by a length of 5 cm.

Surveying of data distribution shows that grades related to 19 investigating parameters do not follow a normal distribution. Bivariate and trivariate logarithmic transformations, and also inverse, box-cox, and Johnson transformations did not work efficiently for normalizing, since final results from calculating W index not only approached zero (Ghannadpour and Hezarkhani, 2015; Ghannadpour et al., 2017a), but significant decrease could be observed (Fig. 18). Moreover, Kolmogorov-Smirnov test also shows that data distribution does not follow normal distribution after applying mentioned transformations.

Since the Spearman correlation coefficient needs less presumptions such as normal distribution of the data, despite more efficiency of the Pearson correlation coefficient, it is applied for calculating the correlation.

8.3. Multivariate Statistical Analysis

8.3.1. Correlation of the Elements

Correlation coefficient between considering variables (i.e. the grade of REEs, U, Th, K and also radioactivity) is calculated in this section for detailed study of their relation. As mentioned in previous section, Spearman correlation coefficient is applied on investigating variables (non-transformed data) in Baghak area that the results are presented in Table 6.

However, in addition to calculating Spearman correlation coefficient, considering minimum values of reported W index for transformed data

by the Box-Cox technique (Fig. 20), the distribution of these data has been assumed ideally as normal and the Pearson correlation coefficient has been calculated for the transformed data and the results are available in Table 6.
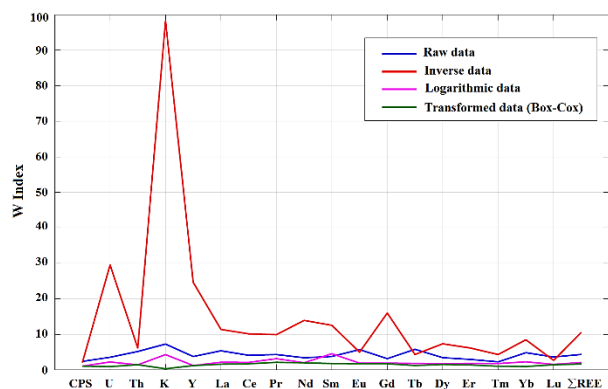

Fig. 18. W Indexes for transformed data.

8.3.2. Separating Anomalous Variables

In this section, correspondent analysis is used to separate anomalous variables (elements) in Baghak mine. Correspondent analysis is a statistical multivariate method, in which simultaneous relation of variables and samples is investigated in one diagram (Cuadras and Cuadras, 2006; Greenacre, 2016). Results from this analysis could be presented in two forms. First, one or several scatter plots are used that it is called factor correspondent analysis. Second, a dendrogram is used and it is called cluster correspondent analysis.

Actually, determining anomalous variables using factor correspondent analysis is targeted in this section. A 151 * 17 matrix named G consisting of REEs and radioactive elements of U, Th, and K is provided as input to the mentioned method. The results of applying this method are based on selecting three eigenvalues from all calculated eigenvalues which cover more than 99% of total variability. Therefore, the study is based on a tri-factor model which is carried out in three scatter plots (Fig. 19 and 20).

As it is shown in Fig. 19, Uranium as an anomalous element has been separated well from the others. In Fig. 20, it is observed that by plotting two factors of F1 and F3, Ce and La joined U and separated themselves from other elements and they are placed far from other REEs and radioactive elements. This shows the separation of U, Ce, and La as anomalous variables from other studying variables. It should be noted that the precision of this separation could be verified based on reported values in Table 5. Since in mentioned table, it could be seen that reported values for U, Ce, and La are much higher than the other investigating values.

8.3.3. Separating Anomalous Samples

In the previous section, anomalous variables (anomalous elements) were determined, while in this section, anomalous samples are separated from background about anomalous elements (U, Ce and La). There are many methods for separating anomaly from background (Khalajmasoumi et al. 2015; Ghannadpour and Hezarkhani, 2016; 2018; Ghannadpour et al. 2017b). In this study, based on the position of the data, U-N fractal method is employed for the purpose (Sadeghi et al. 2012; Hassanpour and Afzal, 2013).

Fig. 21 shows the results of applying the fractal method algorithm (C-N model) to U, Ce and La concentrations.

In the following, the different line segments related to geochemical populations were fitted to the above models in order to define geochemical populations (based on least-square regression). The straight fitted lines can be seen in Fig. 22.

Accordingly, there are four populations for the uranium and five populations for cerium and lanthanum data that were reported in Table 7.

9. Discussion

According to Sangan geology and especially the Baghak anomaly, carbonate rocks aged Cretaceous are mostly dolomite-limestone. Syenogranite to monzonite intrusive bodies and also syenite by the porphyry texture caused skarn and Fe mineralization (magnetite). Results from statistical studies show that the Baghak anomaly due to involving significant amount of U, Ce, La and high concentration of REEs, could be considered as one of the important mines. This fact is also observed well in results from comparative analysis that U, La and Ce as anomalous variables (elements) are separated from other investigating variables.

According to reported values from elemental analysis, prospecting of REEs in this anomaly could be known as dependent to the prospecting method of radiation measurement presented in this study. It was revealed that:

- Reported correlation coefficients between REEs and radioactivity (CPS), uranium and thorium concentration are respectively 0.6, 0.7 and 0.85 which are high and acceptable values.

- The major origin of radioactivity in the study area is uranium, and radioactivity is more affected by this element, and potassium involves less share of radioactivity.

- Decrease of correlation coefficients between REEs and radioactivity (CPS) compared to correlation coefficients between REEs and two elements of U and Th is caused by the K effect on measured radioactivity by spectrometer.

Thus, in statistical studies of results from geochemical analysis of samples taken from Baghak anomaly, it was observed that in addition to the relation of REEs and radioactivity particularly in the case of U and Th in central Iran mineralizations, there is a similar relation in skarn mineralization. The Th concentration in analysis results was reported as low as the background value, but statistical investigating of mentioned results shows that Th despite low concentration in Baghak anomaly, is suitably related to the REEs and little enrichment which is shown along with REEs, states the formation of this element with REEs from the aspect of metallogeny and geochemistry.

Based on geochemical and mineralogical studies and also observing LREE in the allanite structure using SEM, it was concluded about the mineralization of REEs and radioactive elements that REEs have formed as solid solution in silicate minerals particularly allanite which is from the epidote group in a high-temperature phase and probably at the same time with skarn. In other words, REEs especially Ce has substituted Ca due to similar ionic radius in the allanite structure. This also has happened for Th and REEs, but due to low concentration of Th in mineralizing fluids there is no sign of high enrichment. Therefore, little amount of Th along with REEs have placed in silicate network of allanite and explicit relation of radioactive elements and REEs (in addition to such relation in central Iran) is observed in Baghak anomaly mineralization. However, uranium is formed as allanite-independent minerals or in other words, out of silicate network of allanite. Actually, uranium has been mostly trapped as inclusions in empty spaces of allanite and also Fe-bearing minerals, but it is noteworthy that REEs have not been observed in the network of other minerals particularly Fe-bearing minerals (magnetite).

These elements show a thermodynamic behaviour similar to U and Th, and they are solved and moved as different complexes mostly as $REEF3$ and $REECl3$ under deep reduction conditions and low oxygen fugacity, and they are placed as $REEO2$ or $REE2O3$ under oxidation condition in crystal network of minerals located at fluid crystallization end series. REEs are part of large-ion lithophiles and similar to high-reactive lithophile metals like Th, U, P and K. These kinds of elements due to strong ionic bond with oxygen as bivalence and trivalence, are placed in a diverse spectrum of silicate and oxide minerals and scattered in continental crust.

Table 6. Spearman's and Pearson correlation coefficients between rare earth elements and radioactive elements.

	Spearman's correlation coefficients				Pearson correlation coefficients			
	U	Th	K	CPS	U	Th	K	CPS
Y	0.70	0.83	0.50	0.59	0.68	0.86	0.49	0.57
La	0.71	0.83	0.45	0.61	0.73	0.82	0.39	0.60
Ce	0.72	0.86	0.46	0.61	0.73	0.83	0.38	0.60
Pr	0.71	0.88	0.46	0.59	0.68	0.90	0.47	0.57
Nd	0.71	0.89	0.48	0.58	0.66	0.91	0.5	0.56
Sm	0.71	0.90	0.49	0.58	0.69	0.92	0.51	0.57
Eu	0.63	0.86	0.45	0.49	0.65	0.85	0.38	0.48
Gd	0.71	0.89	0.48	0.58	0.69	0.91	0.49	0.57
Tb	0.72	0.87	0.51	0.61	0.72	0.89	0.49	0.61
Dy	0.71	0.87	0.52	0.59	0.70	0.91	0.52	0.58
Er	0.71	0.85	0.54	0.60	0.69	0.88	0.54	0.60
Tm	0.66	0.84	0.57	0.56	0.66	0.86	0.55	0.55
Yb	0.71	0.82	0.59	0.63	0.71	0.85	0.57	0.63
Lu	0.73	0.81	0.6	0.65	0.73	0.82	0.56	0.65
∑ REE	0.71	0.86	0.47	0.60	0.73	0.84	0.39	0.60

Table 7. Baghak mineralization zones based on thresholds of U, Ce and La contents defined from the C-N fractal model.

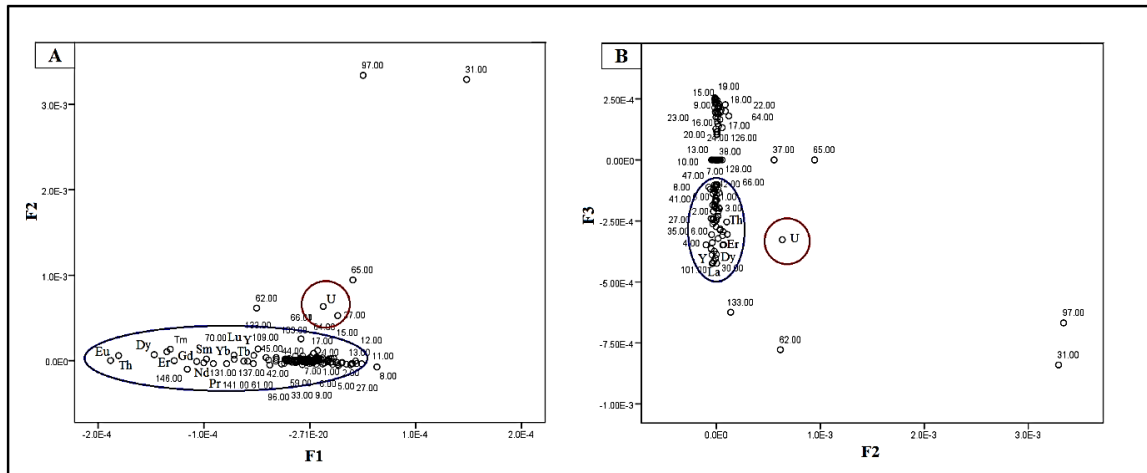| Population	U (ppm)	Fractal dimension (U)	Ce (ppm)	Fractal dimension (Ce)	La (ppm)	Fractal dimension (La)
1	<128.6	0.054	<722	0.08	<700	0.087
2	128.6-202.5	0.614	722-1600	0.586	700-1247	0.623
3	202.5-379.3	2.105	1600-2593	1.404	1247-2073	1.329
4	>379.3	3.841	2593-3300	3.813	2073-3029	3.435
5	-	-	>3300	4.392	>3029	3.619

Fig. 19. Dispersion diagram of derived factors from correspondent analysis method in Baghak mine. A. The first and second factor. B. The second and third factors.
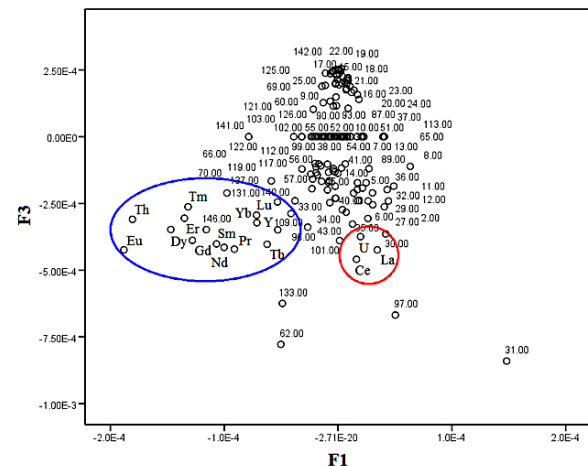

Fig. 20. Dispersion diagram of derived factors from correspondent analysis method in Baghak mine (The first and third factors).

10. Conclusions

Due to the correspondence of the radioactivity trend of the region with the main faults, uranium formations as allanite-independent minerals (as inclusions in empty spaces of Fe-bearing minerals and also allanite) (based on microscopic studies), it could be acknowledged that mineralization of Th and REEs occurred simultaneously with the formation of iron skarn. While uranium mineralization in hydrothermal form occurred in a secondary phase after the skarn iron mineralization.

Results from statistical studies imply anomalous state of U, Ce and La. It was observed that radioactivity in the study area is entirely affected by uranium and REEs show acceptable correlation with radioactivity and consequently uranium. It was also shown that Th despite low concentration has a suitable correlation with REEs due to similar thermodynamic and geochemical behaviour. Therefore, it was concluded from the results that in addition to the presence of relation between REEs and radioactive elements in different areas from central Iran, this relation is explicitly observed in another mineralization type, meaning Sangan skarn iron ore deposit.
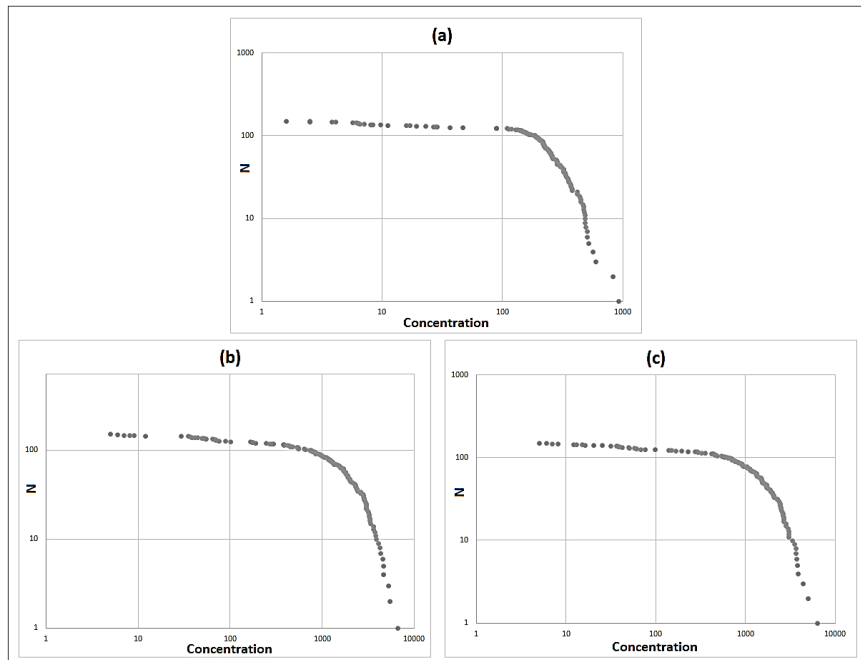
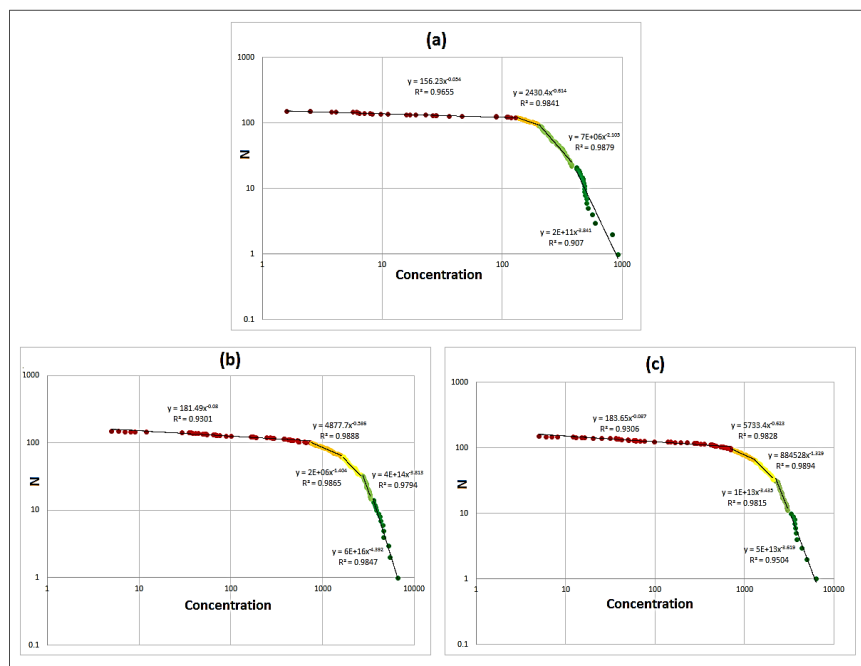**Fig. 21.** C-N log-log plot for concentration of U (a), Ce (b) and La (c).

Fig. 22. The straight fitted lines to geochemical populations of C-N log-log plot for concentration of U (a), Ce (b) and La (c).

Acknowledgment

REFERENCES

[1] Alavi Naini, M., 1982. Geological Quadrangle Map of Khaf: Series Sheet 8059, Ministry of Mines and Metals. Geological survey of Iran, Tehran.

[2] Boomeri, M., 1998. Petrography and geochemistry of the Sangan iron skarn deposit and related igneous rocks, northeastern Iran. PhD thesis, Akita University, Japan, 226 p.

[3] Boomeri, M., 2006. Reare earth elements (REE) in garnet of Sangan iron ore deposit. Geological Society of Iran, Tehran Tarbiat Moallem University, Tehran, Iran. (in Persian)

[4] Cuadras C M, Cuadras D. A parametric approach to correspondence analysis. Linear Algebra and Its Applications, 2006, 417: 64–74.

[5] Ercit, T.S., 2002. The mess that is 'allanite'. The Canadian Mineralogist 40, 1411-1419.

[6] Ghannadpour, S.S., 2014. Geochemical and metallurgical studies of rare earth elements and evaluating their potential in Bafq-Robat Posht-e Badam belt. Atomic Energy Organization of Iran (Under Supervision of I.R.IRAN National Elites Foundation). Tehran, Report, 162 p. (in Persian with English abstract)

[7] Ghannadpour S S, Hezarkhani A. Lead and zinc geochemical behavior based on geological characteristics in Parkam Porphyry Copper System, Kerman, Iran. Journal of Central South University, 2015, 22: 4274–4290.

[8] Ghannadpour S S, Hezarkhani A. Introducing 3D U-statistic method for separating anomaly from background in exploration geochemical data with associated software development. Journal of Earth System Science, 2016, 125(2): 387–401.

[9] Ghannadpour S S, Hezarkhani A, Roodpeyma T. Combination of Separation Methods and Data Mining Techniques for Prediction of Anomalous Areas in Susanvar, Central Iran. African Journal of Earth Sciences, 2017a, 134: 516–525.

[10] Ghannadpour S S, Hezarkhani A, Sharifzadeh M. A method for extracting anomaly map of Au and As using combination of U-statistic and Euclidean distance methods in Susanvar district, Iran. Journal of Central South University, 2017b, 24(11): 2693-2704.

[11] Ghannadpour S S, Hezarkhani A. Providing the bivariate anomaly map of Cu–Mo and Pb–Zn using combination of statistic methods in Parkam district, Iran. Carbonates and Evaporites, 2018, 33(3): 403–420.

[12] Ghannadpour S S, Hezarkhani A, Golmohammadi A. Applying 3D U-statistic method for modeling the iron mineralization in Baghak mine, central section of Sangan iron mines. Geosystem Engineering, 2018, 21(5): 262-272.

[13] Ghannadpour S S, Hezarkhani A. Investigation of geochemical correlation between radioactive and rare earth elements; case study of Baghak mine, NE of Iran. Journal of Mining and Environment, 2021, 12(2): 569-587

[14] Ghannadpour S S, Hezarkhani A. Prospecting Rare Earth Elements (REEs) using radiation measurement; case study of Baghak mine, central Sangan iron ore mine, NE of Iran. Environmental Earth Sciences, 2022, doi:

[15] Golmohammadi, A., Mazaheri, S.A., Karimpour, M.H., Malekzadeh Shafaroudi, A., 2014. Zircon U-Pb dating and geochemistry of Sarkhar and Bermani granitic rocks, East of Sangan iron mine, Khaf. Journal of Petrology 5(17), 83-102. (in Persian with English abstract)

[16] Golmohammadi, A., Karimpour, M.H., Malekzadeh Shafaroudi, A., Mazaheri, S.A., 2013. Petrology and U-Pb zircon dating of intrusive rocks from A, C-south, and Dardvay districts, Sangan iron stone mine, Khaf. Journal of Economic Geology 2(5), 157-174. (in Persian with English abstract)

[17] Golmohammadi, A., Karimpour, M.H., Malekzadeh Shafaroudi, A., Mazaheri, S.A., 2015. Alteration-mineralization, and radiometric ages of the source pluton at the Sangan iron skarn deposit, northeastern Iran. Ore Geology Reviews 65(2), 545-563.

[18] Greenacre M. Correspondence Analysis in Practice. 3th Edition. Chapman & Hall / CRC, Boca Raton, Florida, 2016, 310 p.

[19] Gregory, C.J., Rubatto, D., Allen, C., Williams, I.S., Hermann, J., 2007. Ireland TR. Allanite micro-geochronology: a SHRIMP and LA-ICP-MS study. Chemical Geology 245, 162–182.

[20] Guastoni, A., Nestola1, F., Schiazza, M., 2017. Post-magmatic solid solutions of CaCeAl2 (Fe3+ 2/3□1/3)[Si2O7] [SiO4]O(OH), allanite-(Ce) and REE-bearing epidote in miarolitic pegmatites of Permian Baveno granite (Verbania, central-southern alps, Italy). Mineralogy and Petrology 111, 315–323.

[21] Hassanpour, Sh., Afzal, P., 2013. Application of concentration-number (C-N) multifractal modelling for geochemical anomaly separation in Haftcheshmeh porphyry system, NW Iran. Arabian Journal of Geosciences 6, 957–970.

[22] Iran Eastern Iron Ore Co., 2011. Modelling, type's classification, and calculation of iron deposit in Baghak mine. Report, Sangan Iron Ore Complex.

[23] Khalajmasoumi, M., Lotfi, M., Afzal, P., Sadeghi, B., Memar Kochebagh, A., Khakzad, A., Ziazarifi, A., 2015. Delineation of the radioactive elements based on the radiometric data using concentration–area fractal method in the Saghand area, Central Iran. Arabian Journal of Geosciences 8: 6047–6062.

[24] Malekzadeh Shafaroudi, A., Karimpour, M.H., Golmohammadi, A., 2013. Zircon U-Pb geochronology and petrology of intrusive rocks in the C-North and Baghak districts, Sangan iron mine, NE Iran. Journal of Asian Earth Sciences 64, 256-271.

[25] Mazhari, N., Malekzadeh Shafaroudi, A., Ghaderi, M., 2017. Detecting and mapping different types of iron mineralization in Sangan mining region, NE Iran, using satellite image and airborne geophysical data. Geoscience Journal 21, 137-148.

[26] Mazhari, N., Malekzadeh Shafaroudi, A., Ghaderi, M., 2015. Geology, mineralogy and geochemistry of Ferezneh ferromanganese anomaly, east of Sangan mines complex, NE Iran. Journal of Economic Geology 7(1), 23-37.

[27] Mazhari, N., Malekzadeh Shafaroudi, A., Ghaderi, M., 2016. Geochemistry of intrusive rocks, petrology of skarn, and mineralogy and chemistry of orebodies in Senjedak-I area, east of Sangan mine, Khaf, NE Iran. Scientific Quaterly Journal, GEOSCIENCES 25(100), 235-246. (in Persian with English abstract)

[28] Rabadjieva, D., Tepavitcharova, S., Todorov, T., Dassenakis. M., Paraskevopoulou, V., Petrov, M., 2009. Chemical speciation in mining affected waters: the case study of Asarel-Medet mine. Environmental Monitoring and Assessment 159, 353–366.

[29] Sadeghi, B., Moarefvand, P., Afzal, P., Yasrebi, A B., Daneshvar Saein, L., 2012. Application of fractal models to outline mineralized zones in the Zaghia iron ore deposit, Central Iran. Journal of Geochemical Exploration 122, 9-19.

[30] Sepidar, F., Mirnejad, H., Li, JW., Wei, C., George, LL., Burlinson, K., 2017, Mineral geochemistry of the Sangan skarn deposit, NE Iran: Implication for the evolution of hydrothermal fluid. Chemie der Erde, 77: 399-419.